EFFECT OF INTRA-PLY VOIDS ON THE HOMOGENIZED BEHAVIOR OF A PLY IN MULTIDIRECTIONAL LAMINATES

A. Matveeva[1]*, D. Garoz[2,3], R.D.B. Sevenois[2,3], M Zhu[4], L. Pyl[5], W. Van Paepegem[2], L. Farkas[1]

[1] *Siemens Industry Software NV, Interleuvenlaan 68,3001 Leuven, Belgium*

[2] *Department of Materials, Textiles and Chemical Engineering, Faculty of Engineering and Architecture, Ghent University, Tech Lane Ghent Science Park Campus A, Technologiepark Zwijnaarde 903, B-9052 Zwijnaarde, Belgium*

[3] *SIM Program M3Strength, Technologiepark Zwijnaarde 935, B-9052 Zwijnaarde, Belgium*

[4]*KU Leuven, Department of Materials Engineering, Kasteelpark Arenberg 44, 3001 Leuven, Belgium*

[5]*Department of Mechanics of Materials and Constructions (MeMC), Faculty of Engineering Sciences, Vrije Universiteit Brussel (VUB), Pleinlaan 2, 1050 Brussels, Belgium*

*corresponding author: *anna.matveeva@siemens.com*

Abstract

This work focuses on the effect of intra-ply voids on the homogenized nonlinear behavior of a ply in multidirectional composites. Voids were modeled explicitly on the fiber scale and linked to the ply-scale by the recently developed two-scale framework coupling Classical Laminate Theory on the macro-scale with Finite Element analysis on the micro-scale. Laminates $[\pm 45]_{2s}$ and $[\pm 67.5]_{2s}$ were used as validation cases. The computed homogenized behavior of plies with and without voids for each laminate were compared against existing experimental data on manufactured plates, where the void content is not known. The nonlinearity of the homogenized stress-strain curves of all models is in a very good agreement with experiments up to 1% of applied deformation. The effect of voids was assessed only virtually and it is shown that 4% of void content decreases the ply strength by 30%, transverse stiffness by 8%, whereas longitudinal stiffness, as expected, is not affected by the presence of voids. This work is the first step towards automatization of the virtual identification of the complete set of damage-plasticity parameters for the LMT-Cachan damage model accounting for the presence of intra-ply voids.

1. Introduction

The effect of voids on the mechanical behavior of the fiber reinforced composites, including multidirectional laminates and textile based composites attracts attention of the composite community since many years. A recent review of the effect of voids on the mechanical properties of composites can be found in [1]. One of the main conclusions is that despite the extensive amount of available research, further assessment of the effect of voids is needed. This especially in automotive and aerospace industry, where voids are the key defects in manufacturing techniques such as out-of-autoclave (OoA) and automated tape laying (ATL).

In [2] a multiscale approach to account for effect of voids is presented. The local material properties including transverse strength and Mode I fracture toughness are computed in the presence of voids at the scale of fibers (micro-scale) and then subsequently homogenized to the ply-scale (macro-scale) and assigned to “weak volumes”, representing the presence of voids. Extended Finite Element (XFEM) is

employed at the ply-scale to analyze the crack density evolution in cross-ply laminates with and without the presence of voids. This approach allows to track initiation and propagation of multiple cracks in a ply, as well as to link them to inter-laminar cracks/delamination [3]. The alternative to XFEM, which leads to time-consuming simulations, is to use Continuum Damage Models (CDM) at the ply-scale, where the properties of the ply/or of the region of interest are degraded based on a damage evolution law, which can be modified according to the void content at the lower scale.

A ply damage model developed at LMT-Cachan [4–6] and implemented in the FE code SAMCEF [7] couples the damage evolution in the transverse and in-plane shear direction taking into account the plastic behavior of the reinforced polymer. It is also possible to address the damage evolution in the fiber direction and through-the-thickness. The model has been validated for intra-laminar behavior at the coupon level for UD plies [8]. The model requires several input parameters characterizing elastic behavior, damage, plasticity and final ply failure. The experimental parameter identification requires a special set of experimental tests on different laminates [4, 8, 9]. The effect of voids on the aforementioned parameters has been investigated in [10]. Quasi-static tensile tests on $[90]_8$ and $[0/90]_{2s}$ laminates, as well as cyclic tensile tests on $[\pm 45]_{2s}$ and $[\pm 67.5]_{2s}$ laminates were performed to determine a set of parameters for the LMT-Cachan model for the material under investigation. A clear influence of voids on the damage initiation and propagation and hence on the parameters of the LMT-Cachan damage model was established. Such experimental assessments of the effect of voids is very challenging, especially if to compare the effect against the reference material without voids. By changing the manufacturing parameters, e.g. by lowering the autoclave pressure and the cure temperature, and ensuring the presence of voids in a composite, the behavior of its constituents, mainly the matrix and the fiber/matrix interface might be affected [11]. To decouple the influence of voids from the influence of manufacturing parameters is not a straightforward task. Instead, a virtual parameter identification can offer a promising alternative, however the validation of the methodology is challenging for the same reasons. In [12] Garoz provides a methodology to identify parameters of the Ladevèze damage model by means of dedicated micro-mechanical virtual tests with detailed constituent material models, representative geometry and specific load conditions. In order to verify the approach, Garoz compared the ply model with the identified parameters against the micro-mechanical virtual tests on the $[\pm 45]_{2s}$ and $[\pm 67.5]_{2s}$ laminates. The two approaches gave the same results, except for some small discrepancies in the transverse stress/strain curve of the virtual test on the $[\pm 67.5]_{2s}$ laminate. In the current study, the proposed workflow of Garoz was further modified by considering the presence of voids at the micro-scale level.

To assess the methodology, first, micro-mechanical virtual tests on a void-free material were employed to compare the homogenized behavior of plies in $[\pm 45]_{2s}$ and $[\pm 67.5]_{2s}$ laminates under the static tensile loading against existing experimental data on the laminates. Then, voids were embedded at the micro-scale and their effect on the homogenized behavior of a ply was analyzed only virtually, and not experimentally (the void content in the manufactured plates is not known). Simulation of loading-unloading-reloading of the aforementioned laminates to identify a full set of parameters for the LMT-Cachan damage model is ongoing and not yet presented in this paper.

2. Material and Testing

The composite laminates used in this work are manufactured from unidirectional (UD) prepregs PYROFIL^{TM} TR 360E250S supplied by Honda R&D Co., Ltd and produced by Mitsubishi Chemical Corporation [13]. The prepregs were made of polyacrylonitrile (PAN) based carbon fibers embedded in PYROFIL #360 resin with a volume fraction of 60%. Several plates were made of 8-ply UD prepregs with a stacking sequence $[\pm 45]_{2s}$ and $[\pm 67.5]_{2s}$. The plates were tested under static tension and measured

stress-strain curves served as reference data for modelling results. Several tests on constituents were performed to obtain the input data for the models. The description of all tests is summarized below[1].

Input data identification

- **Fiber properties**

The elastic properties of the carbon fiber are reversed engineere from the 3D homogenized elastic tensor of the UD ply [14]. Full 3D orthotropic elastic stiffness tensor of the ply is computed by measuring the propagation velocity of both the longitudinally and transversally polarized bulk waves at various symmetry planes of a UD Carbon/Epoxy laminate using ultrasonic insonification. Determined Young's moduli, shear moduli and Poisson's ratios can be found in **Table 1**. For the in-depth discussion on the effect of high frequencies produced by the ultrasound on the elastic properties of the material under investigation, the reader is referred to [14].

- **Matrix behavior in tension**

To test the matrix behavior in tension, static tensile tests on the matrix were performed according to the ASTM using a testing machine Instron 5567 with mechanical wedge-type clamps and the test speed 2 mm/min. The tests were accompanied by a mechanical extensometer and a Digital Image Correlation (DIC) Limess VIC 3D system, in 2D mode with one camera. 5 samples were tested, all failing in the gauge section with a brittle failure. The moduli of elasticity were calculated as a slope of the stress-strain curves between 0.1 and 0.3% strain. **Table 1** contains average values and standard deviations of Young's modulus and maximum strain at failure in tension, measured by DIC.

- **Matrix behavior in shear**

To test the matrix behavior in shear, static tensile tests on the matrix were performed according to the ASTM D5379 using a testing machine Instron 5800R with Iosipescu test setup and the test speed 1 mm/min. The tests were accompanied by a DIC system: VIC 3D system, 3D mode with two cameras. The shear modulus was calculated as a maximum progressive slope of the longitudinal stress-strain curve using DIC. **Table 1** contains average values and standard deviation of shear modulus measured by DIC.

- **Interface**

The properties of the interface were not measured for this set of fibers and the matrix. Interfacial strength and toughness are taken from [15] for a similar carbon/epoxy material.

Material properties of the constituents are summarized in Error! Reference source not found..

[1] The presented testing results have been obtained as part of IBO and SBO M3Strength projects, which are part of the research program MacroModelMat (M3).

Table 1. Material properties of constituents

Fibers [14]	
Property	**Value**
Young's moduli	
E_{11} (GPa)	23.3
E_{22} (GPa)	18.4
E_{33} (GPa)	18.4
Poisson's ratio	
ν_{12}(-)	0.02
ν_{13}(-)	0.02
ν_{23}(-)	0.27
Shear moduli	
G_{12} (GPa)	36.9
G_{13} (GPa)	36.9
G_{23} (GPa)	7.2
Fiber radius	
r (mm)	3.6

Matrix	
Property	**Average value (std)**
Young's modulus	
E (MPa)	2.84 (0.1)
Shear modulus	
G (MPa)	0.97 (0.013)
Poisson's ratio	
ν (-)	0.46[a]
Strain at failure in tension	
ε_f^t (%)	2.63 (0.01)
Strain at failure in shear	
γ_f^s (%)	11 (0.03)

Interface [15]	
Property	**Value**
Interface maximum strength	
τ_n(MPa)	50
τ_t (MPa)	75
Interface critical energy release rates	
G_{IC} (N/mm)	0.002
G_{IIC}, G_{IIIC} (N/mm)	0.006
Mixed-mode interaction parameter	
η (–)	1.45

[a] *matrix Poisson's ratio was calculated to fulfil the isotropic assumption of G=E/(2(1+v))*

Data used for validation

UD laminate

Several plates made of 4-ply UD prepregs with a stacking sequence $[0]_4$ and $[90]_8$ were tested under tension to derive longitudinal and transverse Young's moduli of a ply. A testing machine Instron 4505 with mechanical wedge-type clamps and the test speed 2 mm/min was equipped with Instron extensometer and digital image correlation (DIC system): Limess VIC 3D system, 3D mode with two cameras. Transverse modulus in **Table 2** was calculated from results on $[90]_8$ laminate as a slope of the stress-strain curve using DIC between 0.05% and 0.1% strain. Longitudinal modulus in **Table 2** was calculated from results on $[0]_4$ laminate as a slope of the stress-strain curve using DIC between 0.1% and 0.3% strain. DIC Poisson's ration was calculated using DIC response in linear stress-strain curve from the results on $[0]_4$ laminate based on longitudinal and transverse strain available from DIC measurements.

Laminates $[\pm45]_{2s}$ and $[\pm67.5]_{2s}$

Produced laminates with a stacking sequence $[\pm45]_{2s}$ and $[\pm67.5]_{2s}$ were tested according to ASTM D3039. Laminates [±67.5]2s were tested in different loading phases, instead of immediate test to failure. A testing machine Instron 4505 with mechanical wedge-type clamps and the test speed 2 mm/min was equipped with Instron extensometer and digital image correlation (DIC system): VIC 3D system, 3D mode with two cameras. Shear modulus in Table 2 was calculated from results on $[\pm45]_{2s}$ laminate as a slope of the shear stress-strain curve using DIC between 0.2% and 0.6% strain. Measured stress-strain curves are presented in the result section (Figure 5, Figure 6, Figure 7) in a local coordinate system (CS) of a ply, the transformation was done as proposed in [4].

Table 2. Material properties of a UD ply

UD (ASTM + DIC)	
Property	Average value (std)
Young's moduli	
E_{11} (GPa)	127.52 (1.24)
E_{22} (GPa)	8.49 (0.721)
Poisson's ratio	
ν_{12}(-)	0.34 (0.0143)
In-plane shear modulus	
G_{12} (GPa)	4.11 (0.23)
Maximum shear stress	
τ_{12}^{max} (MPa)	52.27 (0.95)
Maximum shear strain	
γ_{12}^{max} (%)	3.66 (0.96)

3. Virtual Material Characterization with the VMC ToolKit

The Simcenter™ VMC ToolKit implemented by Siemens PLM software is a set of software tools developed for virtual material characterization (VMC) to replace physical tests with virtual experiments. The VMC ToolKit allows detailed material modelling at different scales and covers wide range of supported composite types, such as UD plies, 2D/3D woven, non-crimp, weft-knitted, 2D/3D braided fabrics. More detailed concept of the tool can be found in [16]. Several validation cases to predict elastic properties of different composites are demonstrated in [17–19]. Current results are based on the recent extension of the VMC ToolKit towards prediction of non-linear and damage composite behavior accounting for the presence of voids at the fiber scale.

3.1 Micro-scale FE models with the presence of voids

To estimate the "as-manufactured" properties of specimens, *Random Packing* (RP) functionality of the Simcenter™ VMC ToolKit was extended with a feature of *Void Generation* at the fiber scale. The matrix is modeled as a solid body with voids of different shapes (cylindrical and spheroidal) and different sizes. The percentage of voids in the model and their spatial distribution can vary according to the user input. UD fibers remain to have constant diameters and random distribution in the matrix with predefined volume fraction. Melro algorithm [20] was employed to randomly distribute fibers in the matrix with a modification of randomizing the minimum distance between fibers [21].

In the first step, a 2D model is created containing circles with radii of fibers, circles with radii of cylindrical voids and circles with equatorial radii of spheroidal voids. For this step a *random distribution of voids* can be selected as an input method, which will place void centers randomly, keeping a certain space to the boundaries of the unit cell. Radii of circles are chosen randomly within a user defined interval. For the case when exact location of voids and their dimensions are known, e.g. from microCT images, then a manual input of voids using the *Property table* is possible. In this case circles are created according to values, specified in the tables.

In the second step, the 3D model is built. Fibers and cylindrical voids are generated as an extrusion of corresponding circular cross sections through the unit cell thickness and spheroidal voids are revolved according to their equatorial radius (minor radius) and the distance from the center to pole along the symmetry axis (major radius). Through-the-thickness position of spheroidal voids can be defined either randomly or manually as a user input.

Three different configurations of periodic unit cells of randomly distributed fibers in a matrix are generated: matrix being modelled without voids, matrix containing spheroidal voids with void fraction of 2.3% and matrix containing spheroidal voids and cylindrical voids with void fractions of 2.2% and 1.9% respectively (see Figure 1). The cylindrical void was placed in the center of the unit cell with a radius of 3 microns. The size of spheroidal voids was randomly chosen between 1 and 3 microns for both minor and major radii. The dimension of the voids and their volume fractions were chosen randomly from the range of values found in literature [1]. In all cases the size of the unit cell is 38.5 x 38.5 x 3.85 microns, the radius of the fibers is 3.6 microns and the fiber volume fraction is fixed to 60%.

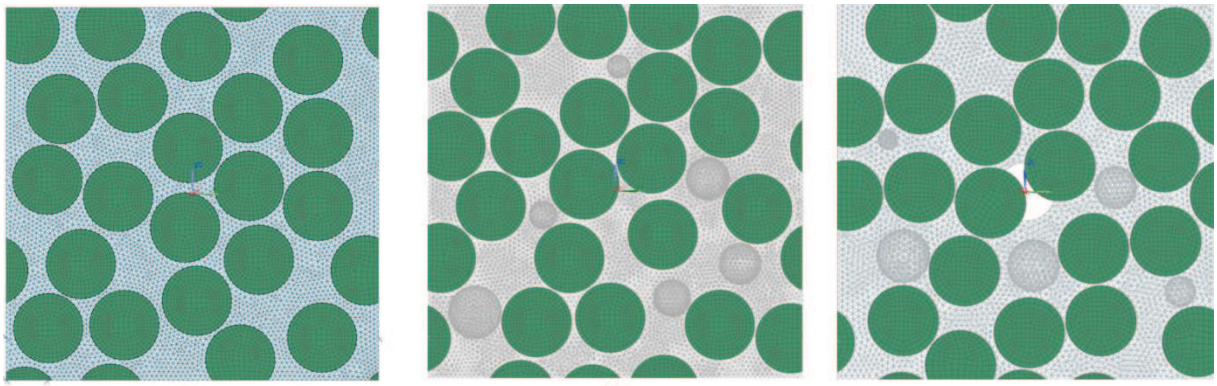

Figure 1 (a) RP model without voids; (b) RP model with 2.3% of spheroidal voids; (c) RP model with 2.2% of spheroidal voids and 1.9% of cylindrical voids.

In all three models, the matrix is discretized using linear 4-node tetrahedal solid elements and fibers using the 8-node hexagonal solid elements, both with a single integration point, linear shape functions and an average element size of 0.5 micron. The interface between fibers and the matrix is modeled by cohesive elements: zero-thickness 8-node hexagonal cohesive elements automatically generated using *Interface Definition* functionality of the VMC ToolKit. Discretization of the unit cells with second order elements and further analysis is under investigation.

The fibers were modeled as transversely isotropic bodies without damage with elastic properties summarized in **Table 1**.

The behavior of the matrix is modeled with elasto-plastic constitutive model available in SAMCEF. The isotropic elastic properties in tension and shear before the yield are listed in **Table 1**. The plastic behavior of the matrix is described with Raghava yield criteria and tabulated engineering stress-strain curve for tension. The ratio between compression and traction limit for Raghava yield criteria is fixed to a default value of 1.3 due to absence of the test data in compression. The damage model for the matrix is a simple model to simulate rupture of the material. Once the equivalent plastic strain has reached the limit, a static damage, d^s, is put to 1 and the true damage is obtained by solving the following law

$\dot{d} = \frac{1}{\tau_c}(1 - \exp(-a_c\langle d^s - d\rangle_+))$, where τ_c and a_c are parameters for the delay law, set to 0.001 and 1, respectively in this work . The elastic Hooke matrix is multiplied by *(1-d)*. The equivalent plastic strain at failure was obtained by comparing the stress-strain curves on a batch test of a pure matrix against experimental data. Considering that the main deformation mechanism of the laminates under

consideration is shear, equivalent plastic strain was obtained by fitting maximum shear strain in simulations with experimental data. For this purpose, due to a big difference in final failure in tension and in shear, the input stress-strain curve in tension was artificially extended up to strain of 11%, which corresponds to the strain at failure of the matrix in shear (Figure 2). This introduces artificial behavior in the unit cell, allowing the unit cell to deform much more in tension than in reality and therefore to reach higher stresses. To overcome this limitation, an application of a different plasticity-damage model for the matrix to be considered.

In the Section 4 it will be shown, that the strain at failure of the matrix set to 11% led to a significant difference in strength of the ply against the experimental curve. One of the possible explanations is that at the micro-scale matrix should be capable to bare larger deformations before the failure. In [22], a matrix tested at the micro-scale shows a much-higher strain to failure than in conventional mechanical setups. Therefore an increased value of strain to failure up to 58% was also considered in this work. This value comes from a different epoxy matrix [19]. Considering the difference in the materials, results obtained with this strain at failure are only indicative.

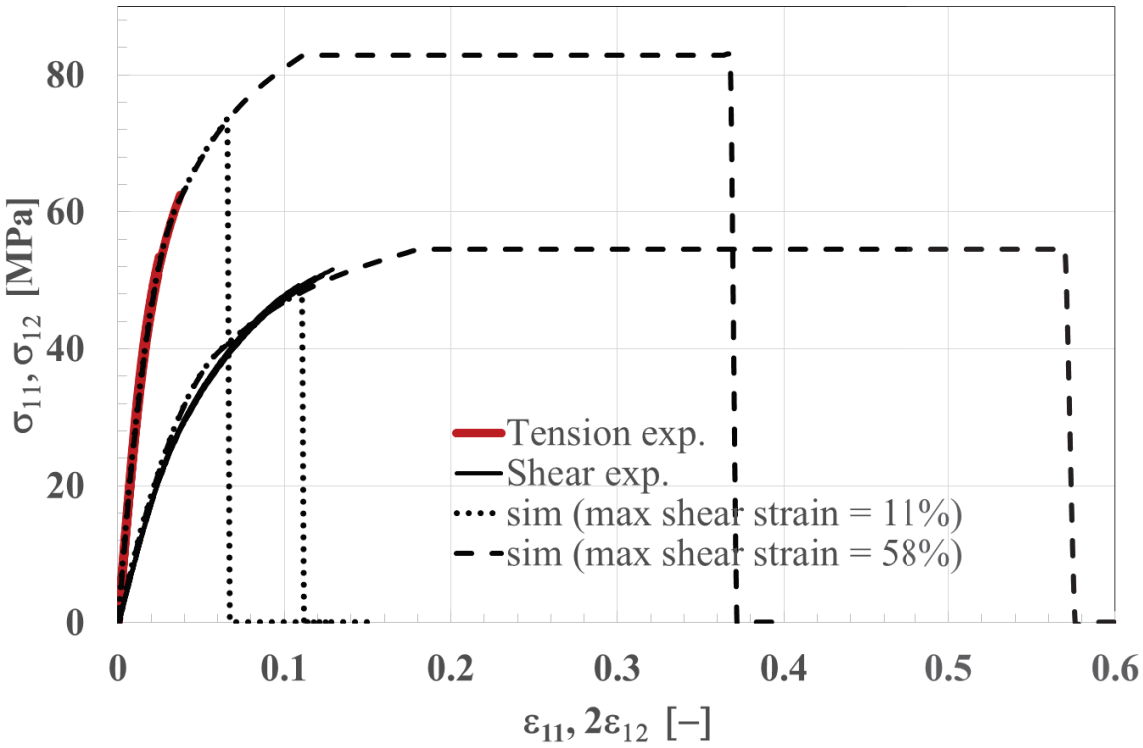

Figure 2 Strain-stress behavior of the epoxy matrix in experiments and simulations for tension and shear

The interface between fibers and the matrix is modelled with a damage interface material model developed in SAMCEF. The cohesive behavior is governed by a damage initiation criterion, damage evolution criterion and a softening law. Both damage initiation and damage evolution criteria are energy-based. The energy threshold was computed as an area of the first triangle of the stress displacement curve based on the known normal and transverse interfacial maximum stresses (**Table 1**) and interfacial stiffness (**Table 3**) considering a bi-triangular traction-separation curve. The elastic interfacial characteristics are chosen by trial-and-error: they should be rather high to model continuity and not too high to avoid numerical divergence. The main principle of the debonding process is after the thermodynamic force across the interface reaches a maximum value of energy threshold, stresses at the interface decrease with increased interfacial separation, indicating a formation of a debonding. Final failure of the interface occurs when the energy release rate reaches its critical value.

Table 3. Input data for the interface material model

Property	Units	Value
Transverse Stiffness (K03)	N/mm^3	2e+07
Shear Stiffness (K02 and K01)	N/mm^3	1.5e+07
Fracture Toughness (GIc, GIIc, GIIIc)	N/mm	0.002 0.006 0.006
Energy Threshold (Y0S)	N/mm	6.25e-05
Coupling Coefficient (DCOU)	-	1.45
! Law Option		Bi-triangular
Time for Delay (TAU)	s.	0.001

3.2 Loading for linear and nonlinear homogenization

To determine both linear and nonlinear homogenized behavior of the material, several analytical and FE-based homogenization schemes are implemented in the VMC ToolKit depending on the model type. This means that depending on the property under consideration, a specific set of loading conditions of the unit cells must be created with a corresponding post processing of mean stresses and strains.

FE-homogenization for stiffness

To compute linear-elastic propertied of a ply, 6 load cases are applied on generated unit cells: 3 in tension and 3 in shear under periodic boundary conditions. The process works also on non-symmetrical meshes, which becomes valuable on complex models [23], [24]. The loading of a unit cell is done by imposing mean strains on a special *Homogenization* element implemented in SAMCEF and dedicated to perform homogenization of a unit cell.

To evaluate the variation in the fiber distribution and in the void content, three configurations for each test case were generated. The average linear-elastic properties and standard deviations are computed and compared with available experimental data.

FE-homogenization of nonlinear behavior

In [12], Garoz developed a process for micro-mechanical tests capturing the damage mechanisms at the micro-scale and specific load conditions, coupled with the Classical Laminate Theory (CLT) on the laminate scale to determine the initiation and propagation of the damage in the ply and to mimic virtual tests on multidirectional laminates. The approach is implemented in the VMC ToolKit. Current implementation is limited to laminates with $[\pm 45]_{2s}$ and $[\pm 67.5]_{2s}$ staking sequence. This is linked to the identification of damage-plasticity material parameters for the LMT-Cachan damage model.

First the CLT is utilized to obtain a link between applied deformations of a laminate in longitudinal direction on the one hand and local strain field in each ply in their local CS on the other hand. Secondly, the ply is modeled as a unit cell with randomly distributed fibers in a matrix, as described in the previous sections and loaded with pre-calculated strains. The load conditions (macro-strains) are introduced using

three dummy nodes per direction x; y; z. Simulating the experimental loading-unloading-reloading is also possible but not considered in this work.

Loading of the unit cell is done with the homogenized element described earlier. Each simulation provides stress-strain fields, from where homogenized stress-strain curves are derived. GUI for the stiffness and damage homogenization are depicted in Figure 3

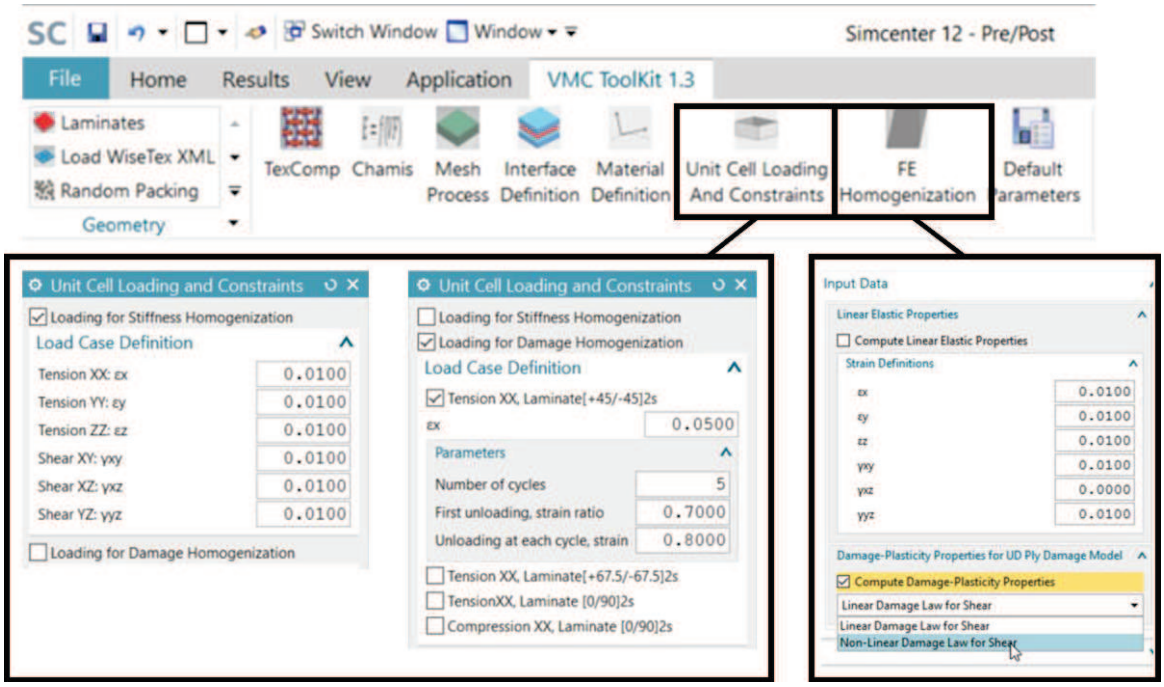

Figure 3 Graphical User Interface of the VMC ToolKit: *Unit Cell Loading and Constraints* and *FE Homogenization*

4. Results

4.1 Patch test on a matrix

The results of the patch test on a one-element model of pure epoxy, loaded in tension and shear with periodic boundary conditions are depicted in Figure 2. The Figure shows a good agreement between experimental and simulated curves in shear up to the failure of the experimental curve. Small discrepancies occur at around 5% of applied shear strain. The final shear strains at failure coincide between the dot-line and experimental data, due to fitting explained in Section 3.1. The nonlinear behavior in tension is identical between simulated and experimental results, since the experimental stress-strain curve in tension was used as input. A larger difference in strain at failure in tension is observed, since the material rupture is described by one value of maximum equivalent plastic strain in both tests, in shear and in tension. Simulated strain at failure in tension is 6.73% for γ_f^s =11% and is 36% for γ_f^s = 58%.

4.2 Effect of voids on the linear elastic properties

Linear Elastic properties were identified for the models with and without voids and compared against the experimental data.

Longitudinal Young's modulus shows a difference of 6.5% between numerical data and experimental measurements. The effect of voids on the Longitudinal Young's modulus is negligible.

Longitudinal shear moduli display only 1% difference between the 0.0%-void simulation and experimental results. The apparent increase of G_{12}-values with an increase in void content is not physical and might be explained by different fiber distributions in models with and without voids. Additionally, there is a difference between in-plane and out-of-plane longitudinal shear moduli in the 0,0%-void model, which should be the same considering the transverse isotropy of a UD ply.

Values for transverse Young's moduli in the 0.0%-void model are higher than the experimental results by 14%. For transverse shear moduli, the experimental data is not available. Both, transverse Young's moduli and transverse shear moduli appear to decrease with void content by 6.6-8.25%. The results on the linear elastic properties are summarized in Figure 4.

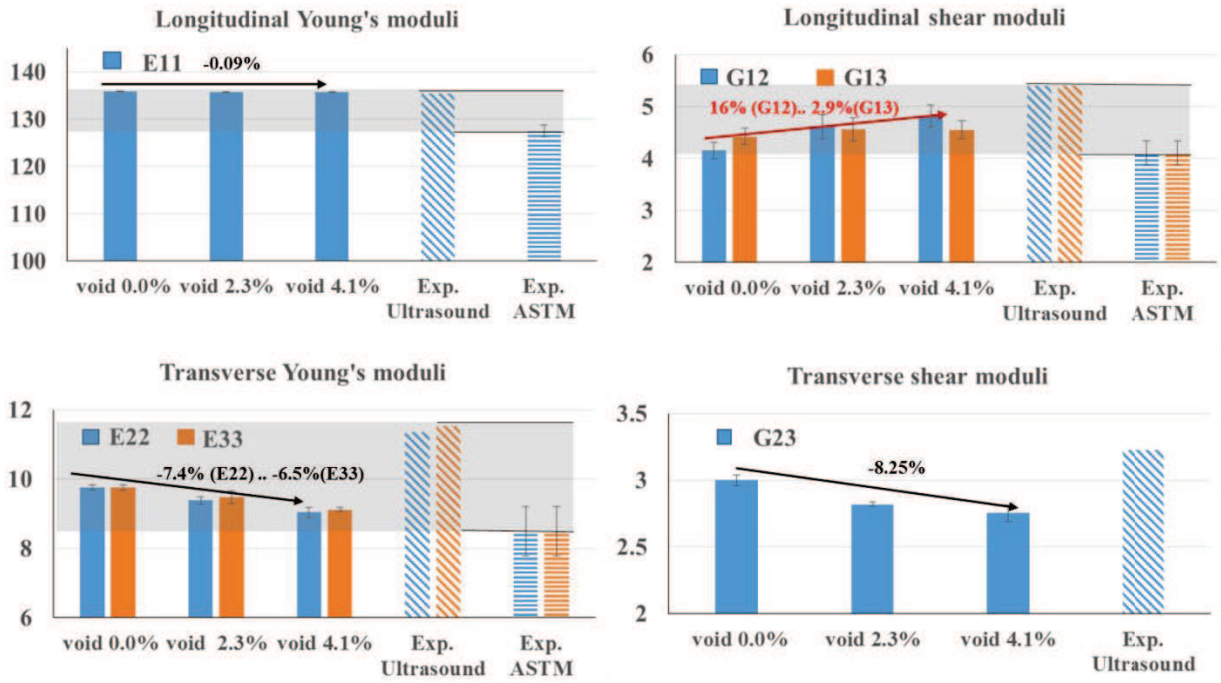

Figure 4 Effect of voids on linear elastic properties of a UD ply

4.3 Effect of voids on nonlinear behavior of a ply

The homogenized stresses across all iterations were extracted from the homogenization element, providing the homogenized curve of a ply in a local CS. Figure 5 contains in-plane shear stress-strain curve of a ply [-45] in a laminate $[\pm 45]_{2s}$ when the shear strain at failure of the matrix was set to 11%. A significant decrease in the maximum stress is observed in comparison with experimental results. The same figure demonstrates the damage development at different values of macro strain of the model

containing 4.1% of voids. Damage in the matrix started in a few locations joining in one crack through the whole model and not as expected at the cylindrical void. The complete failure occurred at around 1.3% driven only by the damage in the matrix and only a few debondings were observed. The damage mechanism in the voidy material shows a step-wise behavior, with the final damage occurring at the same strain as the model without voids.

The maximum stress in the void-free model is 25% higher than in the model containing 4.1% voids.

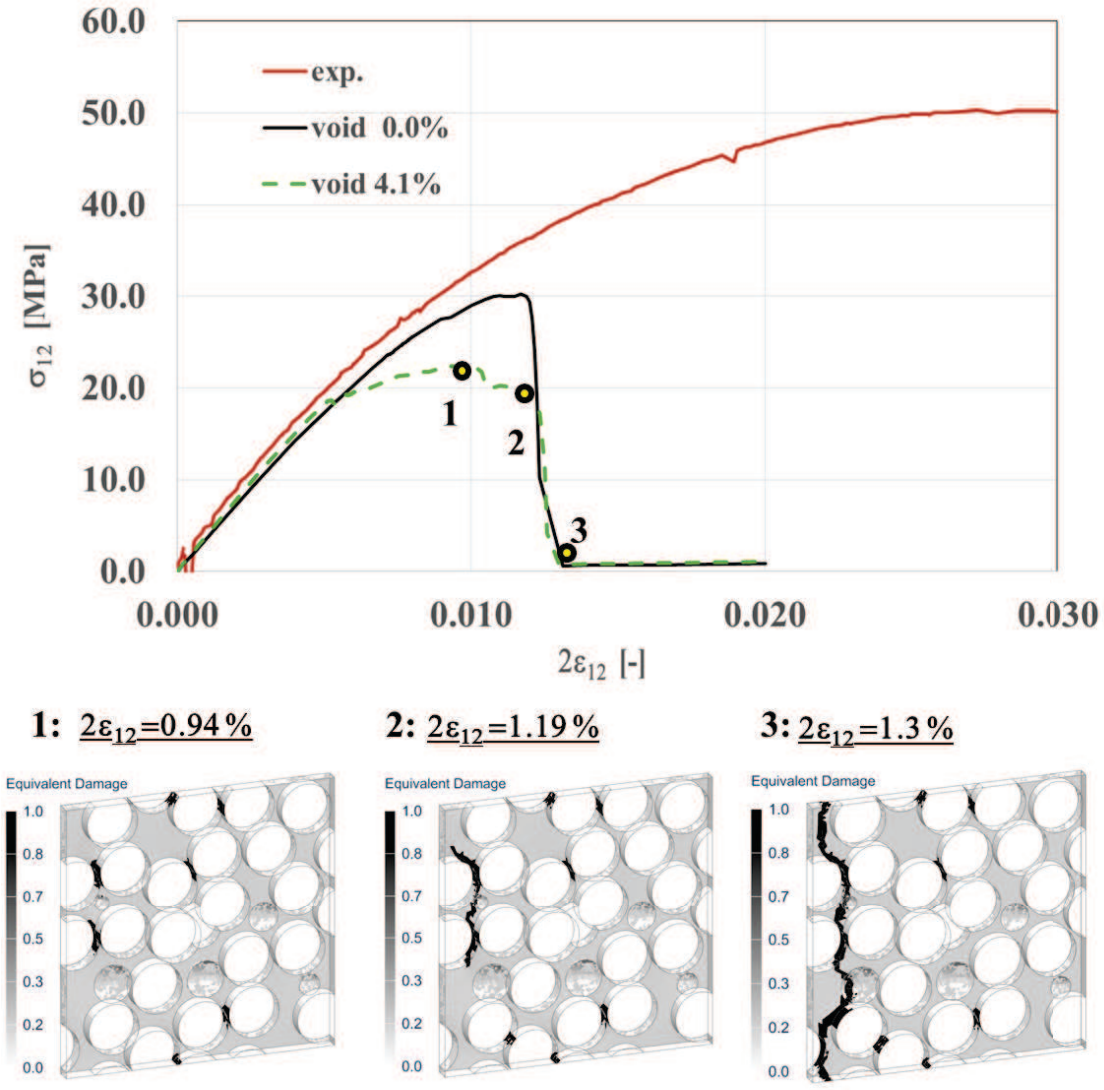

Figure 5 Homogenized stress-strain curves in shear direction in ply [-45] from the virtual test on the $[\pm 45]_{2s}$ laminate (shear strain at failure of the matrix was set to 11%) and damage development in the model containing 4.1% voids

Important to note that generated unit cells represent the behavior of the ply [-45] loaded mainly under shear without taking into consideration the interactions with a ply [+45]. One of the possible reasons that the models with strain to failure of 11% fail so early is because the cracks are not restricted by the neighbouring plies allowing them to progress freely through the structure and causing early failure. Further investigation of this limitation is needed. Another reason for the large discrepancy with the

experimental results, as was mentioned earlier, is that the deformations of the matrix at the micro-scale up to failure can be higher than 11%. To analyze the effect of strain to failure of the matrix on the homogenized behavior of a ply, the following computations are conducted with a strain at failure in a matrix of 58%. Figure 6 presents results of virtual testing on laminates $[\pm 45]_{2s}$. Simulations were not run until the final failure. A similar step-wise behavior can be observed for the model containing voids. The maximum stress value of the model with voids is 30% higher than in the model without voids. For the model containing both cylindrical and spheroidal inclusions, it can be seen that the debonding initiations start around a cylindrical void, at the location of the highest stress concentrations, joining into the transverse crack.

The difference in shear strength between models with 0%, 2% and 4% of void content and experimentally measured strength is 11.7 %, -9.2 % and -20.7 % respectively.

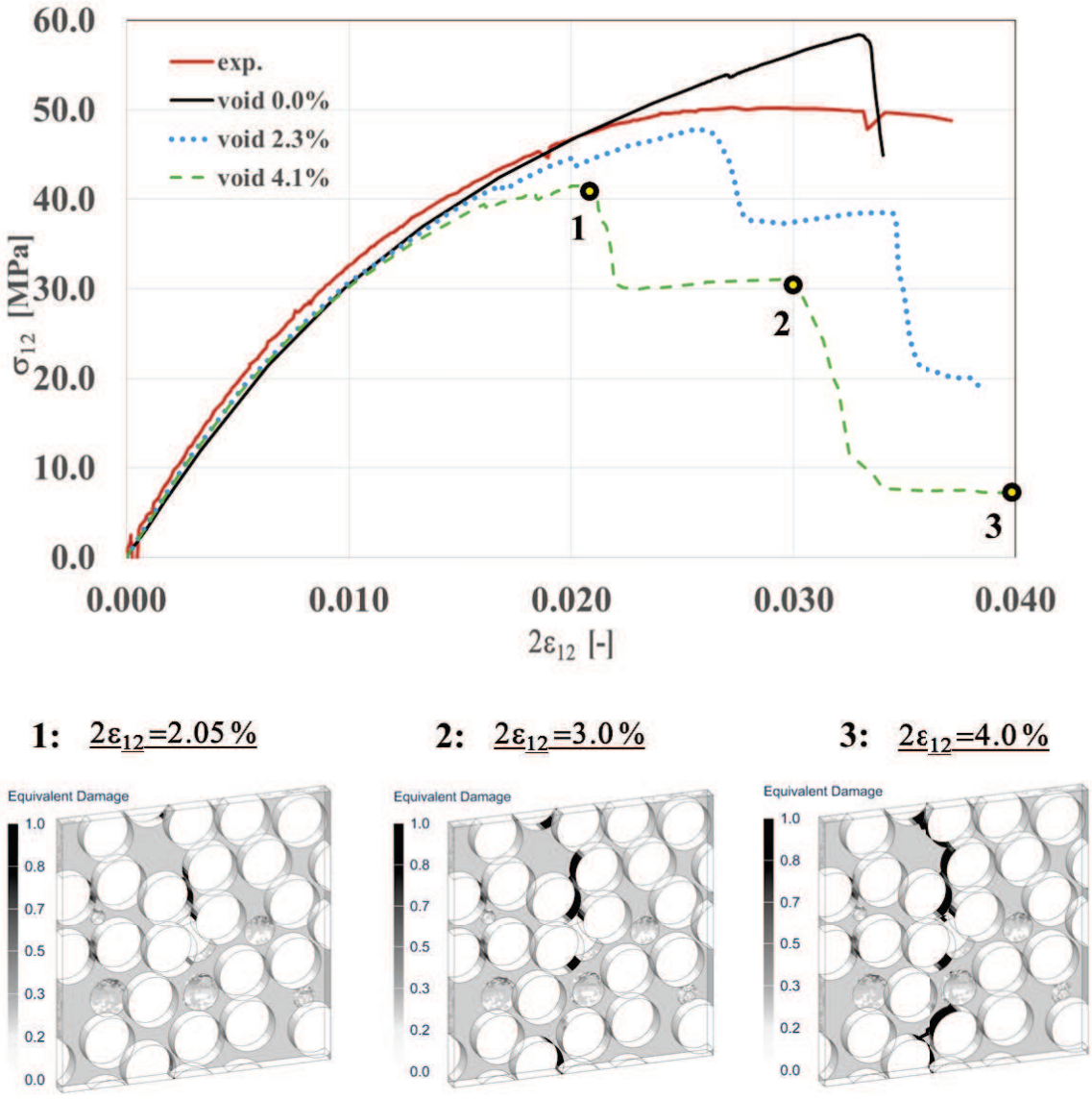

Figure 6 Homogenized stress-strain curves in shear direction in ply [-45] from the virtual test on the $[\pm 45]_{2s}$ laminate (shear strain at failure of the matrix was set to 58%) and damage development in the model containing 4.1% voids

Figure 7 presents results of virtual testing on laminates [+-67.5]. Homogenized stress/strain curves in shear and in transverse direction are compared between all 3 cases and experimental data.

The difference in shear strength between models with 0%, 2% and 4% of void content and experimentally measured strength is 2.6%, 7.6% and -5.4% respectively. The difference in transverse strength between models with 0%, 2% and 4% of void content and experimentally measured strength is 19%, 9.2% and -11.8% respectively.

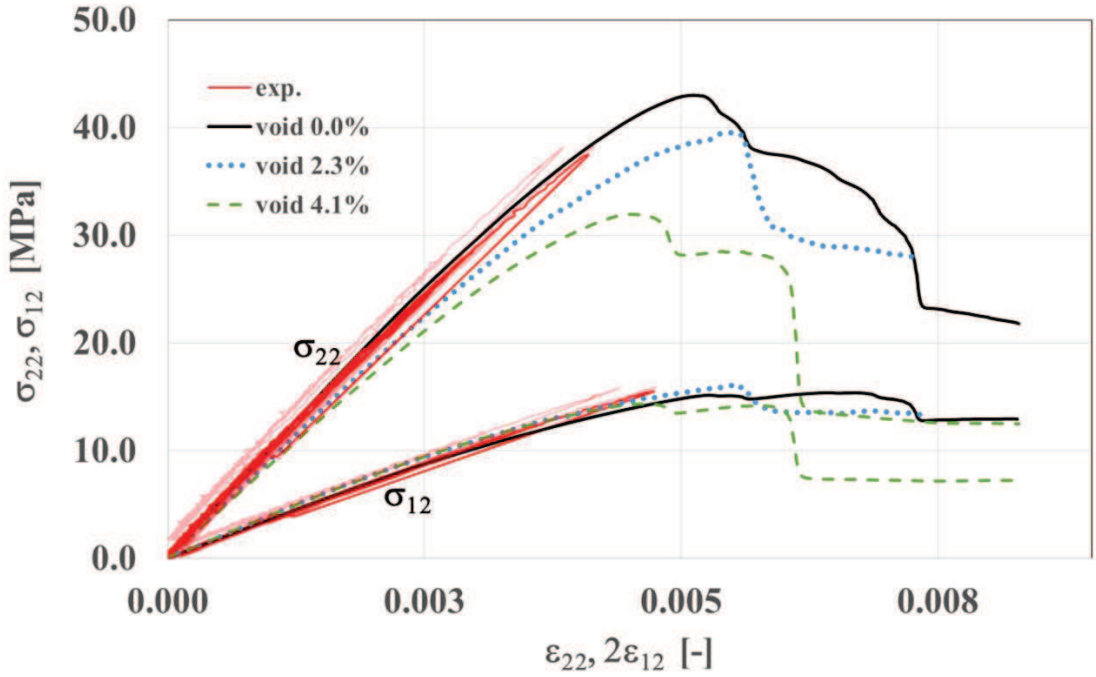

Figure 7 Homogenized stress-strain curves in shear and transverse direction in ply [-67.5] from the virtual test on the $[\pm 67.5]_{2s}$ laminate (shear strain at failure of the matrix was set to 58%).

The summary of maximum ply stresses is presented in Figure 8. The decrease of strength between the void-free model and model with 4.1 % voids is 30% in shear directions for laminate $[\pm 45]_{2s}$ and 25% for laminate $[\pm 67.5]_{2s}$. in transverse direction. The effect of voids on the maximum stresses in shear direction for laminate $[\pm 67.5]_{2s}$ is less pronounced and amounts to 7%.

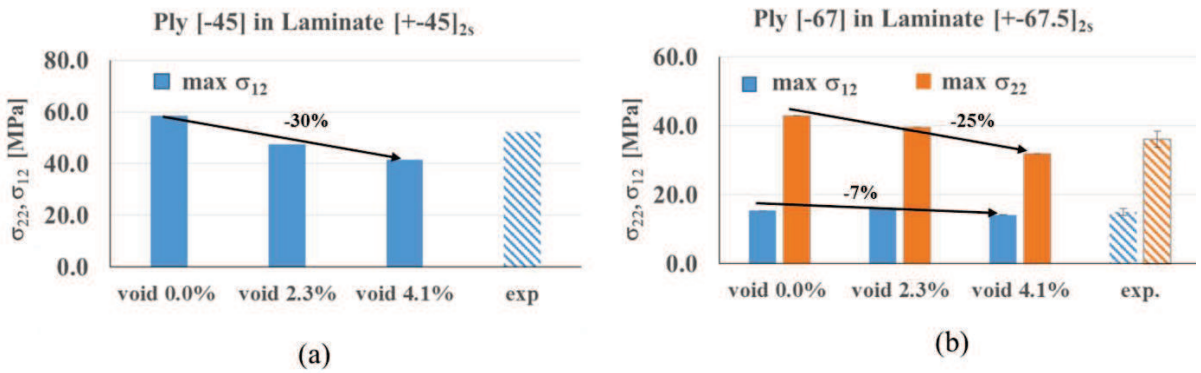

Figure 8 Effect of voids on maximum shear and transverse stress in a UD ply: (a) in ply [-45] from the virtual test on the $[\pm 45]_{2s}$ laminate; (a) in ply [-67.5] from the virtual test on the $[\pm 67.5]_{2s}$ laminate

5. Conclusions and future work

To estimate the "as-manufactured" properties of specimens, the Simcenter™ VMC ToolKit was extended with a feature of void generation at the fiber scale and with a special set of loadings to perform virtual testing on multidirectional laminates. Simulations on the laminates $[\pm 45]_{2s}$ and $[\pm 67.5]_{2s}$ are conducted with and without voids, that are explicitly modeled at the fiber scale with different void type and content. In order to achieve this several unit cells were generated and loaded with a complex macro strain fields, which are computed from deformations of a ply using a CLT.

First, the effect of voids was assessed on the linear elastic properties of the ply. For this, 3 tensile and 3 shear load cases were performed in order to build the full stiffness tensor and to compute linear elastic constants. It is shown that the presence of voids does not affect much the longitudinal elastic properties, and decreases the transversal Young's and shear stiffness by around 8%.

Then the effect of voids was analyzed on the strength/damage of the ply. The effect of the strain to failure of the matrix was also analyzed. The simulation results on a laminate $[\pm 45]_{2s}$ with 11% strain to failure of the matrix, as measured in Iosipescu test, show that the in-plane shear failure of a ply is driven by matrix plastic damage only. In the model containing both cylindrical and spheroidal voids, the damage didn't start at the location of the cylindrical void as expected and maximum stress was only half of experimentally determined values. The in-plane shear failure of a ply with 58% strain at failure of the matrix is initiated by interfacial debonding at the location of a cylindrical void and then dominated by matrix damage. This resulted in a better agreement between virtual tests on laminates $[\pm 45]_{2s}$ and with experiments. Regardless of the strain at failure of the matrix, the introduction of 4.1% of voids led to a decrease of maximum shear stresses in a laminate $[\pm 45]_{2s}$ of approximately 30%. The effect of voids in the laminate $[\pm 67.5]_{2s}$ was assessed only with 58% strain at failure of the matrix, showing the decrease of maximum transverse stresses in a ply by 25% and the decrease of maximum shear stresses in a ply by 8%. The analysis of the effect of voids on the linear elastic properties of a ply shows the decrease of the transverse stiffness by approximately 8% and no effect on the longitudinal properties.

For further improvement of the simulated results, several limitations of the approach need to be addressed. The first is related to the variability of the material. An increase of the longitudinal shear stiffness occurred with increasing void content. This is a clear case of the effect of fiber distribution overriding the effect of voids. A higher number of test cases for each void-content needs to be considered to increase the reliability of the results. The second limitation is the application of periodic boundary conditions on the micro-scale models, which results in a periodic repetition of the damage across the ply. Therefore, numerical results presented here should not be treated as absolute values, because the ply cracking considering crack evolution would affect the predicted maximum stresses. The assessment of this limitation will be considered for further improvement of the VMC ToolKit towards efficient identification of a complete set of damage-plasticity parameters for the LMT-Cachan damage model accounting for the presence of intra-ply voids and towards virtual testing on multidirectional laminates in general.

Acknowledgments

The authors gratefully acknowledge SIM (Strategic Initiative Materials in Flanders) and VLAIO (the Agency Flanders Innovation & Entrepreneurship) for their support of the IBO project M3Strength (Grant no.140158), which is part of the research program MacroModelMat (M3), coordinated by Siemens (Siemens PLM Software, Belgium).

6. References

[1] Mehdikhani M, Gorbatikh L, Verpoest I and Lomov S V 2018 Voids in fiber-reinforced polymer composites: a review on their formation, characteristics, and effects on mechanical performance *J. Compos. Mater. In print*

[2] Mehdikhani M, Petrov N A, Straumit I, Melro A R, Lomov S V and Gorbatikh L 2018 The effect of voids on matrix cracking in composite laminates revealed through combined modeling at the micro- and meso-scales *In preparation*

[3] Petrov N A, Gorbatikh L and Lomov S V 2017 A parametric study assessing performance of eXtended Finite Element Method in application to the cracking process in cross-ply composite laminates, *Composite Structures*. **187**, 489-497

[4] Ladevèze L and LeDantec E 1992 Damage modelling of the elementary ply for laminated composites," *Composites science and technology*, **43**(3), 257–267

[5] Ladevèze P 1992 A damage computational method for composite structures, *Computers and Structures*, **44**, 79–87

[6] Ladevèze P, Allix O, Gornet L, Lévêque D and Perret L 1998 A computational damage mechanics approach for laminates: Identification and comparison with experimental results, *Damage Mechanics in Engineering Materials*, 481–500

[7] Delsemme J P, Bruyneel M, Jetteur P, Magneville B, Naito T and Urushiyama Y 2015 Progressive damage modeling in composites: from aerospace to automotive industry, *Proc* in *Third Int. conf. on Buckling and Post-buckling Behavior of Composite Laminated Shell Structures,* p 22-26, Braunschweig, Germany

[8] Bruyneel M, Delsemme J, Goupil A, Jetteur P, Lequesne C, Naito T and Urushiyama Y 2014 Damage modeling of laminated composites: validation of the intra-laminar law of SAMCEF at the coupon level for UD plies," in *Proc of the 16th European conf. on composite materials*, Seville, Spain

[9] Malgioglio F, Carella-Payan D, Magneville B and Farkas L 2016 Parameter Identification for interlaminar damage modelling of composites, *In Proc of the 6th ECCOMAS Thematic Conf. on the Mech. Response of Composites,* Eindhoven, Netherlands

[10] Steensels E 2017 Mechanical damage in carbon fibre-reinforced composites: experimental observations and model validation, *Maser Thesis, K.U. Leuven*

[11] Mehdikhani M, Standaert A, Steensels E, Vallons K, Gorbatikh L and Lomov S. V 2018 Multi-scale digital image correlation for detection and quantification of matrix cracks in carbon fiber composite laminates in the absence and presence of voids, *Compos. Part B-eng. under review.*

[12] Garoz D, Gilabert F A, Sevenois R D B, Spronk S W F and Van Paepegem W 2017 Material parameter identification of the elementary ply damage mesomodel using virtual micro-mechanical tests of a carbon fiber epoxy system, *Composite Structures*, **181**, 391–404

[13] Mitsubishi Chemical Corporation, https://www.m-chemical.co.jp/en/index.html

[14] Sevenois R D B, Garoz D, Verboven E, Spronk S W F, Gilabert F A, Kersemans M, Pyl L and Van Paepegem W 2018 Multiscale Approach for Identification of Transverse Isotropic Carbon Fibre Properties and Prediction of Woven Elastic Properties using Ultrasonic Identification, *under review*

[15] Arteiro A, Catalanotti G, Melro A, Linde P and Camanho P 2014 Micro-mechanical analysis of the in situ effect in polymer composite laminates, *Comp. Struct,* **116**, 827–840

[16] Farkas L, Vanclooster K, Erdelyi H, Sevenois R D B, Lomov S V, Naito T, Urushiyama Y and and Van Paepegem W 2016 Virtual material characterization process for composite materials: an industrial solution," in *Proc. of the 17th European. Conf. on Composite Materials ,p* 26–30, *Munich*

[17] Catera P G, Gagliardi F, Mundo D, De Napoli L, Matveeva A and Farkas L 2017 Multi-scale modeling of triaxial braided composites for FE-based modal analysis of hybrid metal-composite gears," *Comp. Struct.*, **182**, 116–123

[18] Matveeva A, Tabatabaei A, Sevenois R D B, Farkas L, Van Paepegem W and Lomov S V 2017 Assessement of different meso-modelling techniques for 2D woven composites, *in Proc* of the *NAFEMS conf : Multiscale and Multiphysics Modeling & Simulation - Innovation Enabling Technologies, At Columbus, OH*, USA
[19] Shishkina O, Matveeva A, Wiedemann S., Hoehne K, Wevers M, Lomov S V, Farkas L 2018 X-Ray Computed Tomograhy-based FE-Homogenization of sheared organo sheets, in *Proc. of the 18th European Conf. on Composite Materials, Athens, Greece*
[20] Melro A, Camanho P and Pinho S 2008 Generation of random distribution of fibres in long-fibre reinforced composites, *Comp. Science and Technology,* ***68****,* 2092–2102
[21] Romanov V, Lomov S V, Swolfs Y, Orlova S, Gorbatikh L and Verpoest I 2013 Statistical analysis of real and simulated fibre arrangements in unidirectional composites, *Composites Science and Technology*, **87**, 126–134
[22] X. Morelle 2015 Mechanical characterization and physics-based modeling of highly-crosslinked epoxy resin, PhD Thesis, UCL-Université Catholique de Louvain, Belgium
[23] Garoz D, Gilabert F A, Sevenois R D B, Spronk S. W. F and Van Paepegem W 2018 Consistent Application of Periodic Boundary Conditions in Implicit and Explicit Finite Element Simulations of Damage, t*o be submitted*
[24] Kassem G. A. 2009 Micromechanical material models for polymer composites through advanced numerical simulation techniques, *PhD Thesis*, RWTH Aachen University